Journal of Magnetic Resonance 250 (2015) 1–6

Contents lists available at ScienceDirect

Journal of Magnetic Resonance

journal homepage: www.elsevier.com/locate/jmr

Zero-field nuclear magnetic resonance spectroscopy of viscous liquids

Y. Shimizu [a,b], J.W. Blanchard [c,d,*], S. Pustelny [a], G. Saielli [e], A. Bagno [f], M.P. Ledbetter [a], D. Budker [a,g,h], A. Pines [c,d]

[a] Department of Physics, University of California at Berkeley, CA 94720-7300, United States
[b] Department of Physics, Graduate School of Science, Nagoya University, Furo-cho, Chikusa-ku, Nagoya 464-8602, Japan
[c] Department of Chemistry, University of California at Berkeley, CA 94720, United States
[d] Materials Sciences Division, Lawrence Berkeley National Laboratory, Berkeley, CA 94720, United States
[e] CNR Institute on Membrane Technology, Padova Unit, Via Marzolo, 1, 35131 Padova, Italy
[f] Department of Chemical Sciences, University of Padova, Via Marzolo, 1, 35131 Padova, Italy
[g] Nuclear Science Division, Lawrence Berkeley National Laboratory, Berkeley, CA 94720, United States
[h] Helmholtz-Institut Mainz, Johannes Gutenberg University, Germany

ARTICLE INFO

Article history:
Received 21 July 2014
Revised 11 October 2014
Available online 1 November 2014

Keywords:
Zero-field NMR
Scalar coupling
Density functional theory
Viscous liquids

ABSTRACT

We report zero-field NMR measurements of a viscous organic liquid, ethylene glycol. Zero-field spectra were taken showing resolved scalar spin–spin coupling (*J*-coupling) for ethylene glycol at different temperatures and water contents. Molecular dynamics strongly affects the resonance linewidth, which closely follows viscosity. Quantum chemical calculations have been used to obtain the relative stability and coupling constants of all ethylene glycol conformers. The results show the potential of zero-field NMR as a probe of molecular structure and dynamics in a wide range of environments, including viscous fluids.

1. Introduction

Recent developments in zero- and ultra-low-field (ZULF) NMR with superconducting quantum interference devices (SQUIDs) [1–3] and atomic magnetometers [4–7] open new possibilities for imaging and spectroscopy. In conventional NMR spectroscopy, chemical shifts and spin–spin couplings are utilized to distinguish molecular structures [8,9], where spin–spin couplings are treated as a first-order perturbation to the Zeeman energy. To obtain high sensitivity and resolution of chemical shifts, high magnetic fields are conventionally used, requiring expensive radio-frequency spectrometers and bulky superconducting magnets with cryogenic cooling. ZULF-NMR with atomic magnetometers utilizing alkali-atom vapor cells has enabled non-cryogenic, desktop spectroscopy [5–7]. While chemical shifts vanish at zero field, ZULF-NMR spectra are governed by indirect nuclear spin–spin couplings called scalar or *J*-couplings that depend on the electronic structure and geometry of the molecule [5,10]. In contrast to the chemical shift due to diamagnetic current of the occupied orbitals, the *J*-coupling is an indirect interaction between nuclear spins through second-order hyperfine effects [8,9,11–13], and thus serves as a sensitive local probe of molecular geometry and electronic structure.

Until now, investigations of ZULF-NMR with atomic magnetometers have focused on low-viscosity liquids with simple molecular structures and weak intermolecular interactions [5–7], achieving half width at half maximum as low as ≈0.01 Hz [14–16] comparable to that of advanced high-field (HF) NMR. Many materials of practical interest – polymers or proteins, for example, feature significant van der Waals interactions and hydrogen bonds. Therefore, the ability to detect such interactions through their *J*-coupling spectra in ZULF-NMR is of significant importance. Compared to HF-NMR, ZULF-NMR may have advantages in resolution because of the absence of the static and dynamic broadening mechanisms inherent in the spectroscopy of chemical shifts. For a liquid sample, the linewidth of ZULF-NMR is governed by the dynamical width due to nuclear dipole fields and *J*-coupling [9]. However, the magnitude of *J*-couplings sensitively depends on the molecular conformation and interactions in a way that is not always straightforward to predict.

Here we use a model system, $^{13}C_2$-labeled ethylene glycol (EG, HO–$^{13}CH_2$–$^{13}CH_2$–OH), featuring strong intermolecular hydrogen bonds. NMR has been utilized to investigate molecular dynamics [17,9,18] and conformational equilibria of polyalcohols [19–26]. Among ten non-equivalent isomers of EG with different dihedral

* Corresponding author at: Department of Chemistry, University of California at Berkeley, CA 94720, United States.
E-mail address: jwblanchard@berkeley.edu (J.W. Blanchard).

http://dx.doi.org/10.1016/j.jmr.2014.10.012
1090-7807/

angles in one C–C and two C–O torsion angles, theoretical calculations have shown that two *gauche* conformers with a C–C torsion angle at possible potential minima, 60° and 300°, are favorable rather than *trans* conformers with a torsion angle of 180° [27–35]. The two-bond *J*-couplings in ^{1}H NMR measurements support the predominant *gauche* state [19–26]. However, NMR studies of EG have been usually made in solution states [19–26] possibly due to the broadening of NMR spectra in neat EG, and the effect of intermolecular hydrogen bonding between EG molecules for the conformations remains insufficiently explored.

In this paper, we study the effect of viscosity on ZULF- and HF-NMR spectra by controlling the viscosity through varying temperature and water content of EG solutions. We observe changes in ZULF-NMR spectra that are due to minute changes in *J*-couplings that can be attributed to intermolecular hydrogen bonding and molecular dynamics in bulk EG.

2. Experimental technique

The ZULF-NMR apparatus has been described previously in Ref. [7] and references therein. An EG sample pre-polarized in a permanent 2.0 T magnet situated outside the magnetic shield was shuttled to the zero-field region through a guiding coil. Because the low frequencies of ZULF-NMR preclude the use of inductive detection, NMR signals were detected with an atomic magnetometer incorporating a Rb vapor cell (^{87}Rb and 1300 torr N_2) operating at 180 °C. The alkali vapor was optically polarized with circularly polarized light tuned to the D1 transition. Magnetic field measurements were performed by continuously monitoring optical rotation of linearly polarized light, propagating in a direction perpendicular to the pump beam, tuned about 100 GHz away from the center of the pressure broadened D1 transition. Optical rotation of the probe beam was monitored by using a balanced polarimeter or by using a polarimetry scheme involving a quarter-wave plate/photoelastic modulator and a crossed polarizer. In the latter case, phase sensitive detection was used. ZULF-NMR transient signals were collected for 4–12 s following application of a ~1 ms duration magnetic-field pulse to excite nuclear spin coherences. For the measurements presented here, 256 or fewer transients were averaged prior to Fourier transformation. The sample temperature was controlled by flowing hot air and monitored with a thermocouple.

NMR measurements were performed with bulk EG (1,2-^{13}C ethanediol from Sigma Aldrich with 1–2% water content as measured by Karl-Fischer titration) and dilutions with distilled water in a 5 mm diameter Pyrex tube. The materials were used without further purification. The volume of EG was 100 μL for the undiluted sample and 50 μL for aqueous solutions. NMR tubes were sealed with parafilm to reduce evaporation and absorption of water. The spectra were obtained by Fourier transformation of the free-decay signals after cancellation of phase independent external noise (e.g., that from power lines) and subtraction of thermal-drift signals of the magnetometer. To obtain the linewidth and shift of spectral peaks, the ZULF spectra were fitted to a sum of Lorentzians.

3. Computational method

The optimized structure of each of the ten conformers was obtained via energy minimization including second-order Møller–Plesset correlation energy corrections [36] and using a triple-ζ quality correlation-consistent basis set augmented with diffuse functions (MP2/aug-cc-pVTZ). Solvent reaction field of chloroform (dielectric constant $\varepsilon = 4.7$) and ethylene glycol ($\varepsilon = 37.7$) was included by means of the polarisable continuum model [37]. Electronic energies were corrected with the addition of enthalpy and entropy corrections at 298 K to obtain the Gibbs free energies. Subsequent calculations of *J*-couplings, also in the presence of the solvent reaction field, were run using density functional theory with the BHandH functional [38] and the pcJ-2 basis set [39], which is specifically tailored for the calculation of spin–spin couplings. All contributions to *J* were included: the Fermi-contact, diamagnetic and paramagnetic spin–orbit and spin–dipole terms. All calculations were run with the Gaussian09 software package [38]. Following Ref. [40], we label each structure with three letters representing the HOCC, OCCO and CCOH dihedral angles. Lower case g, g′, t indicate values around +60°, −60° and 180°, respectively, while uppercase G and T refer to the gauche or trans OCCO conformation, respectively. Figures are shown in Supporting Information. Degeneracy of the conformers was taken into account in the calculation of the population distribution and weighted average *J*-couplings.

4. Results and discussion

The thermal variations of internuclear interactions were studied by ZULF-NMR spectra of bulk ethylene glycol. Fig. 1 shows ZULF-NMR spectra at temperatures from 30 to 108 °C. To understand

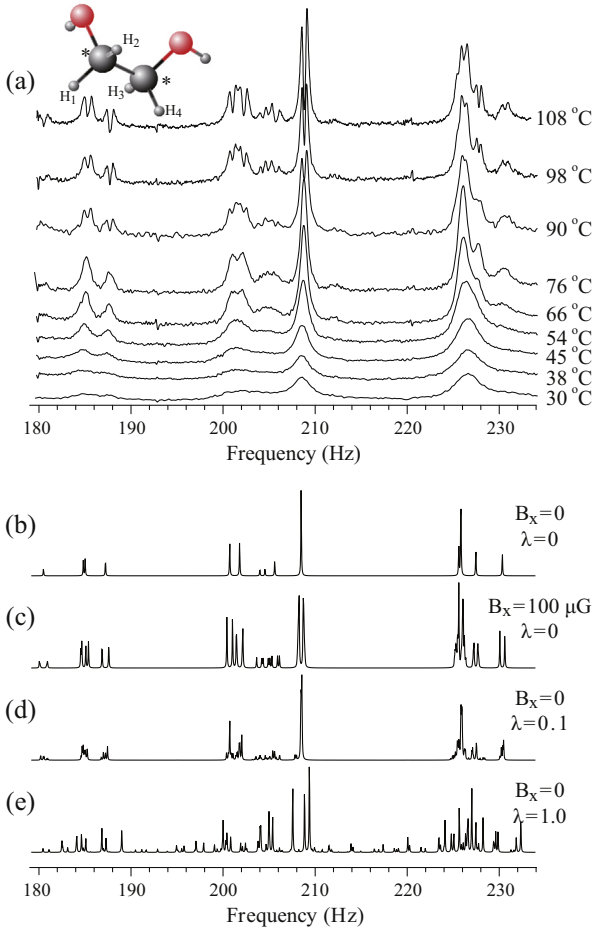

Fig. 1. (a) Temperature dependence of the ZULF-NMR spectrum of bulk $^{13}C_2$-ethylene glycol. The vertical axis is the Fourier transformed lock-in signal. The inset figure shows molecular structure of ethylene glycol (gauche conformer) where * denotes ^{13}C, small spheres: H atoms; intermediate spheres: O. (b) Simulation of 76 °C spectrum without couplings to hydroxyl protons at zero magnetic field. (c) Spectral simulation without couplings to hydroxyl protons in the presence of a 100 μG field. (d) Spectral simulation with couplings to hydroxyl protons scaled by $\lambda = 0.1$ at zero magnetic field. (e) Spectral simulation including full couplings to hydroxyl protons ($\lambda = 1$) at zero magnetic field. Simulated spectra are shown with narrow linewidth (extended relaxation time) in order to reveal fine structure.

these spectra, we first note that an isolated $^{13}CH_2$ group produces a signal at $(3/2)^1J_{CH}$ [5], corresponding to ≈210 Hz. In EG, two such groups are coupled together via one-bond carbon–carbon coupling $^1J_{CC}$, a two-bond proton–carbon coupling $^2J_{CH}$, and two inequivalent three-bond proton-proton couplings $^3J_{HH,1} = J(H_1, H_3) = J(H_2, H_4)$ and $^3J_{HH,2} = J(H_1, H_4) = J(H_2, H_3)$. These additional couplings produce the rich splitting patterns shown in Fig. 1.

The profile is in qualitative agreement with the simulation obtained from the time-evolution of the density matrix for six spin-1/2 nuclei [5] evaluated with the values of the coupling constants obtained from HF NMR [25]. The simulated *J*-coupling spectra at 76 °C, as shown in Fig. 1(b and c), were obtained using the following values: $^1J_{CH}$ = 141.2 Hz, $^1J_{CC}$ = 40.0 Hz, $^2J_{CH} = -2.0$ Hz, $^3J_{HH,1}$ = 4.0 Hz, and $^3J_{HH,2} = 5.9$ Hz. To simulate the potential effects of slow hydroxyl proton exchange, additional simulations were performed, as shown in Fig. 1(d and e), using the calculated values: $^3J_{HOH} = 5.40$ Hz, $^2J_{COH} = -3.45$ Hz, $^3J_{COH} = 5.03$ Hz, $^4J_{HOH} = 0.02$ Hz, and $^5J_{(OH)(OH)} = 0.12$ Hz, with these couplings scaled by a dimensionless parameter λ (λ = 0 implies no coupling to the hydroxyl protons due to fast exchange and λ = 1 implies full coupling, as would be the case in the absence of hydroxyl exchange). Comparison between the simulations and the experimental spectra in Fig. 1 suggests that all couplings to hydroxyl protons are averaged to zero by chemical exchange. The vicinal proton coupling, $^2J_{HH}$, has no observable effect on the spectrum [25].

As the temperature is increased beyond 90 °C, an additional doublet structure becomes apparent for each line with a splitting of 0.7 Hz. We attribute this splitting to an external magnetic field that appears due to imperfect residual-field shimming at elevated temperatures, consistent with Fig. 1(c). Note that the linewidth of the ZULF spectra decreases with increased temperature (Fig. 2). While the linewidth exceeds 2 Hz full width at half-maximum at room temperature, we have $\delta\nu = 0.30$ Hz at 108 °C. As seen in Fig. 2(b), $\delta\nu$ follows the viscosity [41] as a function of temperature. The narrowing with increasing temperature is likely due to enhanced molecular tumbling [17]. The linewidth may also be affected by hydroxyl proton exchange, which leads to relaxation via modulation of *J*-coupling frequencies, as discussed in Ref. [10]. Together with the line narrowing, the spectral intensity increases due to reduced relaxation during shuttling, reflecting an increase of the spin–lattice relaxation time.

In addition to the appearance of extra structures with increasing temperature, the spectra exhibit a slight positive shift, e.g. from 208.65(5) at 38 °C to 208.92(1) Hz at 108 °C for the central intense peak, as shown in Fig. 2(a). The position of this peak is primarily determined by the sum of $^1J_{CH}$ and $^2J_{CH}$, which may provide information about the conformational equilibrium, though a rigorous means of extracting all coupling constants from the ZULF spectrum would provide stronger support.

To examine the effect of solution concentration on molecular conformation, we measured ZULF-NMR for aqueous EG solutions with different concentrations, as shown in Fig. 3. We find narrowing of ZULF-NMR spectral features, similar to what is observed in the thermal variation for the bulk sample. Presumably, this reflects the reduction of the correlation time of molecular rotations with both increasing temperature and dilution, improving the averaging of the dipole–dipole interactions that broaden the lines.

Each line shows an approximately parallel shift to higher frequency with increasing water content, keeping the interval between the lines approximately constant. A parallel shift of the spectrum would indicate that the effect is due to $^1J_{CH}$, though deviations from a perfectly parallel shift would indicate that effects are due to changes in $^2J_{CH}$. The much larger shift (1.8 Hz between 2% and 80%, Fig. 4(a)) compared to the thermal shift in neat EG (≈ 0.3 Hz between 40 and 110 °C, Fig. 2(a)) highlights the importance of the solvent effects.

Dilution with water exponentially suppresses the viscosity (Fig. 4(c)) and also tends to replace hydrogen bonds among EG molecules with those to water. The linewidth also scales as viscosity, as observed in the temperature dependence, indicating the correlation time of molecular tumbling governs the linewidth. In contrast to the thermal variation, an offset linewidth of 0.3 Hz (the left vertical axis) remains in the scaling relation, presumably due to the effect of water protons in the infinite-dilution limit. This linewidth is substantially greater than would be attributed to magnetic field inhomogeneity or temperature gradients (approximately 0.01 Hz) [14–16], and should be primarily representative of the intrinsic spin–spin relaxation time.

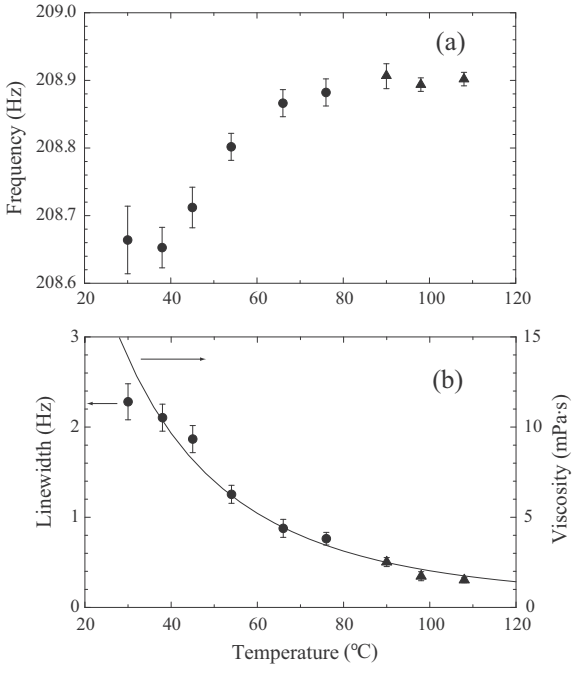

Fig. 2. (a) Central resonance frequency and (b) its linewidth plotted against temperature for bulk $^{13}C_2$-ethylene glycol. The data shown by closed triangles are obtained from fitting with two Lorentzians with the same fixed intensities for a doublet; the averaged frequency of a doublet is plotted for 90 °C and above. The solid line in (b) shows temperature dependence of viscosity, and is not a fit.

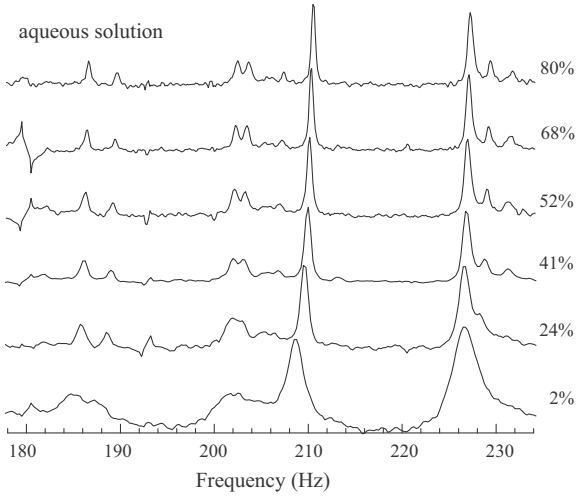

Fig. 3. ZULF NMR spectra for aqueous solutions of $^{13}C_2$-ethylene glycol as a function of water content (wt.%) measured at 36 °C. The intensity is normalized by the maximum intensity at each concentration.

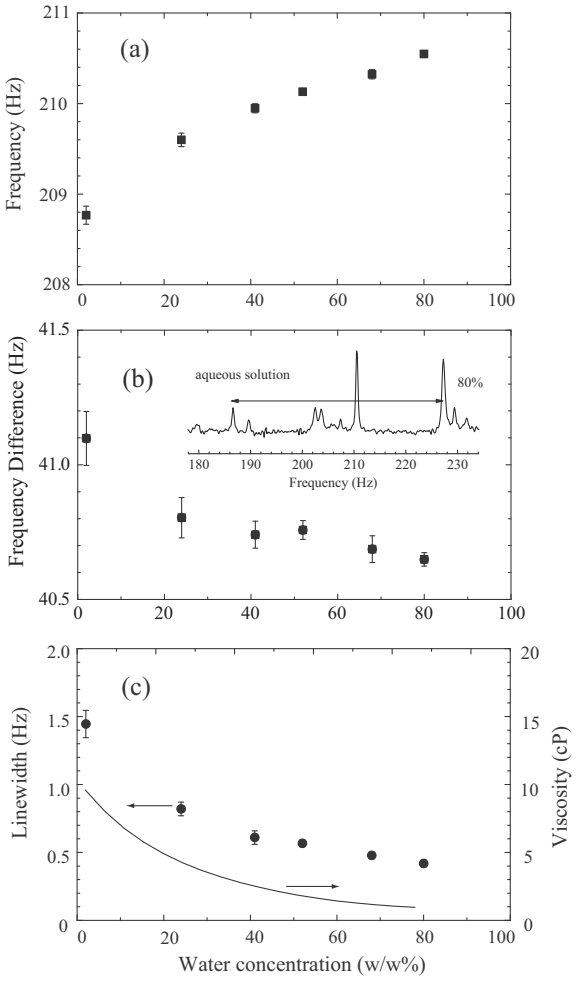

Fig. 4. (a) Central-resonance frequency, (b) multiplet width proportional to $^1J_{CC}$, and (c) the central-resonance linewidth vs. the concentration of aqueous $^{13}C_2$-ethylene glycol solution. The solid curve in (c) shows viscosity data for the aqueous solution [41].

A detailed understanding of the shifts towards higher frequencies observed both with increasing temperature and dilution with water would require an accurate description of the conformers' populations. Molecular-dynamics simulations would be able, in principle, to provide the full distribution of dihedral angles of EG. However, currently available classical force fields are not sufficiently accurate to describe hydrogen bonds and the associated key dihedral angles involving the OH groups (indeed, there is no generally accepted parameterization even of the OCCO angle [30,42,43]). On the other hand, Car–Parrinello simulations [44] are too demanding for the slow dynamics of a viscous fluid. Thus here we only attempt to provide a qualitative description.

To this end it is convenient first to examine the simpler case of EG in chloroform ($CHCl_3$), where intermolecular interactions, especially H bonds, are expected to play a negligible role. The experimental data from the literature are compared with the results of DFT calculations where the EG molecule is embedded in a continuous medium with the dielectric constant of $CHCl_3$ (see Section 3). This case serves as a test of the performance of the theoretical level selected. We then compare the experimental data here reported with the results of DFT calculations where the dielectric constant has been set to the value in EG in order to model long range solvent effects in the neat liquid. However, explicit intermolecular H bonds cannot be fully described by this method.

The results of the calculations in chloroform are summarized in Table 1. For each conformer there are 28 couplings which are reduced to 10 independent values because of fast rotation and/or molecular symmetry. In Table 1, we only report the averaged values; for example $^1J_{CH}$ is the average of four calculated couplings of each ^{13}C with its two protons.

In agreement with previous theoretical investigations, [40,45] the most stable conformer is tGg′ followed by gGg′ and g′Gg′, which account for about 90% of the total. Most G conformers exhibit some intramolecular hydrogen bonding (HB), as expected for an essentially isolated molecule. The Boltzmann-averaged J values can be directly compared with those reported in [25] measured in $CDCl_3$, because this solvent is expected to have negligible HB with the solute EG. The agreement is good, especially for the couplings involving ^{13}C: the average absolute error is just 0.37 Hz, which gives us confidence on the calculated population distribution in $CHCl_3$.

Calculated couplings using the solvent reaction field of EG differ only slightly from those in $CHCl_3$; this is not unexpected because, even though the calculations include the long-range dielectric response of the environment, no explicit solvent molecules account for intermolecular HB. However, in EG, solvent intermolecular hydrogen bonds are not negligible and may change the relative conformer stability, although the experimental results in Table 2 do not show striking differences compared with the experimental values of Table 1.

The experimental value of $^1J_{CH}$ in neat EG at room temperature (≈141.2 Hz) is slightly lower than in $CDCl_3$. This suggests that the population distribution in bulk EG is different from what we have calculated using EG as a solvent, and, because of intermolecular interactions, likely enriched in some conformers with low values of $^1J_{CH}$, such as gGg, tGg or tGt, to remain within G conformers.

Table 1
Calculated J-coupling constants for ethylene glycol conformers in chloroform. The expectation values for each coupling constant at 298 K are weighted by fractional conformer populations, obtained in terms of the relative energies and degeneracies. Experimental values taken from Ref. [25]. Coupling constants involving hydroxyl protons are included in the Supporting Information.

	$^1J_{CH}$ (Hz)	$^1J_{CC}$ (Hz)	$^2J_{CH}$ (Hz)	$^2J_{HH,1}$ (Hz)	$^3J_{HH,2}$ (Hz)	Degeneracy	ΔG (kcal/mol)	%Pop
g′Gg′	140.4	39.9	−1.0	3.0	6.5	2	0.28	14.8
gGg′	141.2	38.0	−1.3	3.2	6.8	4	0.36	25.9
gGg	139.4	38.0	−0.8	2.8	7.1	2	1.59	1.6
gTg′	141.5	41.1	−3.8	12.6	6.2	2	1.82	1.1
gTg	141.6	41.1	−3.8	12.6	6.1	2	1.96	0.9
tGg′	141.5	39.8	−2.0	2.9	6.7	4	0.00	47.9
tGg	139.5	40.8	−1.7	2.1	7.0	4	1.72	2.6
tGt	139.8	43.2	−2.6	1.7	6.9	2	1.45	2.1
tTg	141.9	43.6	−4.6	12.3	6.3	4	1.79	2.3
tTt	142.1	46.1	−5.3	12.0	6.3	1	1.65	0.7
$\langle J\rangle_{298K}$	141.2	39.6	−1.8	3.4	6.7			
J_{exp}	141.6	39.3	−1.6	2.6	6.4			

Table 2
Calculated *J*-coupling constants for ethylene glycol conformers in ethylene glycol. The expectation values for each coupling constant at 298 K are weighted by fractional conformer populations, obtained in terms of the relative energies and degeneracies. Experimental values are taken from this work. Coupling constants involving hydroxyl protons are included in the Supporting Information.

	$^1J_{CH}$ (Hz)	$^1J_{CC}$ (Hz)	$^2J_{CH}$ (Hz)	$^3J_{HH,1}$ (Hz)	$^3J_{HH,2}$ (Hz)	Degeneracy	ΔG (kcal/mol)	%Pop
g′Gg′	140.8	39.9	−1.1	2.9	6.6	2	0.30	12.2
gGg′	141.7	38.1	−1.3	3.2	6.8	4	0.20	28.6
gGg	140.0	38.6	−0.8	2.4	7.0	2	1.12	3.1
gTg′	141.9	41.2	−3.8	12.6	6.2	2	1.59	1.4
gTg	141.9	41.2	−3.8	12.5	6.1	2	1.62	1.3
tGg′	142.0	39.7	−2.0	3.0	6.7	4	0.00	40.4
tGg	140.3	40.8	−1.7	2.2	6.9	4	1.09	6.4
tGt	140.6	43.0	−2.6	1.9	6.9	2	1.06	3.4
tTg	142.1	43.5	−4.6	12.3	6.3	4	1.64	2.6
tTt	142.2	46.0	−5.3	12.1	6.3	1	1.60	0.7
$\langle J\rangle_{298K}$	141.6	39.6	−1.8	3.7	6.7			
J_{exp}	141.2	40.0	−2.0	4.0	5.9			

The magnitude of $^2J_{CH}$ is also slightly larger in neat EG than in $CDCl_3$, also likely due to stabilization of conformers with more negative values of $^2J_{CH}$ due to intermolecular interactions. The variations in these values may explain the small shift towards higher frequencies as the temperature is increased because the frequency of the central resonance is, to first order, $\frac{3}{2}(^1J_{CH} + {}^2J_{CH})$. If the conformers with smaller values of $^1J_{CH} + {}^2J_{CH}$ are more stabilized by intermolecular interactions in bulk EG, an increase in temperature would produce an increase in the average value and therefore a shift of the central resonance of the ZULF spectrum. A similar rationale may explain the even larger shift observed when EG is diluted in water, even though a precise determination of the various conformers population in EG and the exact values of their couplings, is not possible.

It is noteworthy that the C–C coupling constant is also strongly dependent on the EG conformation. As a general rule, and similarly to the $^1J_{CH}$ case, we note that G conformers exhibit smaller $^1J_{CC}$ couplings (38–41 Hz) while T conformers exhibit larger $^1J_{CC}$ (41–45 Hz) couplings. A rough measure of the strength of this coupling is given by the width of the "multiplet" centered around $\frac{3}{2}(^1J_{CH} + {}^2J_{CH})$. As shown in Fig. 4(b), the spectral features move slightly together with increasing dilution, indicating a decrease in $^1J_{CC}$.

5. Conclusions and outlook

In this work, intermolecular interactions were studied with ZULF-NMR in ethylene glycol, a prototypical viscous liquid. For a bulk sample we observed relatively broad *J*-coupling spectra with reduced intensity compared to low-viscosity liquids. The linewidth of the ZULF spectral features varies in the same way as viscosity does in the thermal and the aqueous concentration dependences. We observed small changes in the *J*-coupling constants while controlling the influence of intermolecular interactions with heating and dilution. The results are consistent with high-field NMR studies.

Overall, density functional theory calculations successfully model the conformer distribution and *J*-couplings in EG, provided that they are experimentally determined under conditions where intermolecular interactions are weak (i.e., in chloroform). When such interactions are strong (bulk EG or aqueous solution), we expect the population of conformer to be altered. Nevertheless, the agreement between calculations and experiment is still quite good. Therefore, the capability of accurately measuring *J*-couplings by ZULF-NMR, coupled with their computational predictions, can provide information on the conformer distribution.

Our results illustrate the capability of ZULF-NMR for determining molecular structures and conformations in viscous liquids with significant intermolecular interactions and fast relaxation. The linewidth of ZULF-NMR can be free from inhomogeneous fields and chemical shift anisotropy, and is thus a straightforward method for the measurement of intrinsic relaxation times. Future work focusing more closely on hydrogen bond interactions may be feasible using strong bases to suppress hydroxyl exchange, as in Ref. [25].

Application of ZULF-NMR to non-liquid samples such as gels and polymers is an interesting direction for further investigation. ZULF-NMR may be particularly useful for the study of anisotropic materials, as the spin–spin interaction tensors are not truncated by large magnetic fields, allowing for the measurement of so-called "non-secular" terms. In combination with multi-dimensional and decoupling techniques, applications to more complex biologically relevant molecules are also the goals of ZULF-NMR. However, for materials with relaxation times shorter than 0.5 s, prepolarized nuclear spins become unpolarized during the shuttling process to the zero-field region. Further technical improvements (e.g., faster shuttling) will be necessary for application to solid systems with fast relaxation rates.

Acknowledgments

This work has been supported in part by the National Science Foundation under Award CHE-1308381 (D. Budker), by the U.S. Department of Energy, Office of Basic Energy Sciences, Division of Materials Sciences and Engineering under Contract No. DE-AC02-05CH11231 (A. Pines, and J.W. Blanchard), and by Grant-in-Aid for Scientific Research (Nos. 25610093 and 23225005) and Institutional Program for Young Researcher Overseas Visits from JSPS (Y. Shimizu). D.B. acknowledges the support of the Miller Institute for Basic Research in Science. J.W.B. is also supported by a National Science Foundation Graduate Research Fellowship under Grant No. DGE-1106400. S.P. acknowledges the support from the National Centre for Research and Development within the Leader Program. Calculations were run on the Linux cluster of the Laboratorio Interdipartimentale di Chimica Computazionale (LICC) of the Department of Chemical Sciences of Padova. G.S. thanks the STM-CNR 2013 program for sponsoring his visit to LBNL. We also thank Dr. István Pelczer at the Princeton University Department of Chemistry for assistance in obtaining high-field NMR spectra, Prof. C. Austen Angell at Arizona State University for the use of his laboratory's Karl-Fischer titrator, and Dr. Ralph Page at UC Berkeley for helpful discussions.

Appendix A. Supplementary material

The supplemental information includes the high-field NMR of bulk $^{13}C_2$-ethylene glycol, and additional computational details.

Supplementary data associated with this article can be found, in the online version, at http://dx.doi.org/10.1016/j.jmr.2014.10.012.

References

[1] Y.S. Greenberg, Application of superconducting quantum interference devices, Rev. Mod. Phys. 70 (1998) 175.
[2] R. McDermott, A. Trabesinger, M. Muck, E. Hahn, A. Pines, J. Clarke, Liquid-state nmr and scalar couplings in microtesla, Science 295 (2002) 2247.
[3] M.P. Ledbetter, G. Saielli, A. Bagno, N. Tran, M.V. Romalis, Observation of scalar nuclear spin–spin coupling in van der Waals complexes, Proc. Nat. Acad. Sci. 109 (2012) 12393.
[4] D. Budker, M. Romalis, Atomic magnetometer, Nat. Phys. 3 (2009) 227.
[5] M. Ledbetter, C. Crawford, A. Pines, D. Wemmer, S. Knappe, J. Kitching, D. Budker, Optical detection of NMR *J*-spectra at zero magnetic field, J. Mag. Res. 199 (2009) 25.
[6] T. Theis, P. Ganssle, G. Kervern, S. Knappe, J. Kitching, M.P. Ledbetter, D. Budker, A. Pines, Parahydrogen-enhanced zero-field nuclear magnetic resonance, Nat. Phys. 7 (2011) 571.
[7] M.P. Ledbetter, T. Theis, J.W. Blanchard, H. Ring, P. Ganssle, S. Appelt, B. Blumich, A. Pines, D. Budker, Near-zero-field nuclear magnetic resonance, Phys. Rev. Lett. 107 (2011) 107601.
[8] R.R. Ernst, G. Bodenhausen, A. Wokaun, Principles of Nuclear Magnetic Resonance in One and Two Dimensions, Clarendon Press, Oxford, UK, 1987.
[9] E.D. Becker, High Resolution NMR, third ed., Academic Press, New York, 2000.
[10] S. Appelt, F.W. Hasing, H. Kuhn, B. Blumich, Phenomena in *J*-coupled nuclear magnetic resonance spectroscopy in low magnetic fields, Phys. Rev. A 2007 (2007) 023420.
[11] E. Hahn, D. Maxwell, Chemical shift and field independent frequency modulation of the spin echo envelope, Phys. Rev. 84 (1951) 1246.
[12] E.B. McNeil, C.P. Slichter, H.S. Gutowsky, "Slow beats" in F^{19} nuclear spin echoes, Phys. Rev. 84 (1951) 1245.
[13] N.F. Ramsey, E.M. Purcel, Interaction between nuclear spins in molecules, Phys. Rev. 85 (1952) 143.
[14] J.W. Blanchard, M.P. Ledbetter, T. Theis, M.C. Butler, D. Budker, A. Pines, High-resolution zero-field NMR *J*-spectroscopy of aromatic compounds, J. Am. Chem. Soc. 135 (2013) 3607.
[15] M. Emondts, M.P. Ledbetter, S. Pustelny, T. Theis, B. Patton, J.W. Blanchard, M.C. Butler, D. Budker, A. Pines, Long-lived heteronuclear spin-singlet states in liquids at a zero magnetic field, Phys. Rev. Lett. 112 (2014) 077601, http://dx.doi.org/10.1103/PhysRevLett.112.077601.
[16] M.P. Ledbetter, S. Pustelny, D. Budker, M.V. Romalis, J.W. Blanchard, A. Pines, Liquid-state nuclear spin comagnetometers, Phys. Rev. Lett. 108 (2012) 243001, http://dx.doi.org/10.1103/PhysRevLett.108.243001.
[17] N. Bloembergen, E. Purcell, R. Pound, Nuclear magnetic relaxation, Nature 160 (1947) 475.
[18] D. Kruk, A. Herrmann, E. Rossler, Field-cycling NMR relaxometry of viscous liquids and polymers, Prog. Nucl. Magn. Reson. Spectrosc. 63 (2012) 33–64.
[19] T.M. Connor, K.A. McLauchlan, High resolution nuclear resonance studies of the chain conformation of polyethylene oxide, J. Phys. Chem. 69 (1965) 1888.
[20] K. Pachler, P. Wessels, Nuclear magnetic resonance study of 2-fluoroethanol and ethylene glycol, J. Mol. Struct. 6 (1972) 471.
[21] I.N.D.Y. Han, A.J. Woo, S. Hong, Molecular conformation of hydrogen-bonded ethylene glycol in sodalite: a ^{1}H CRAMPS NMR, IR, and ^{2}H NMR study, J. Phys. Chem. B 106 (2002) 6206.
[22] S.R. Salman, R.D. Farrant, P.N. Sanderson, J.C. Lindon, Conformation of ethane-1,2-diol from analysis of gradient-enhanced inverse detection, Magn. Reson. Chem. 31 (1993) 585–589.
[23] G. Chidichimo, D. Imbardelli, M. Longeri, A. Saupe, Conformation of ethylene glycol dissolved in a nematic-lyotropic solution: an NMR analysis, Mol. Phys. 65 (1988) 1143.
[24] C. Pearce, J. Sanders, Improving the use of hydroxyl proton resonances in structure determination and NMR spectral assignment: inhibition of exchange by dilution, J. Chem. Soc. Perk. Trans. 1 (1994) (1994) 1119.
[25] K. Petterson, R. Stein, M. Drake, J. Roberts, An NMR investigation of the importance of intramolecular hydrogen bonding in determining the conformational equilibrium of ethylene glycol, Magn. Reson. Chem. 43 (2005) 225.
[26] J.S. Lomas, ^{1}H NMR spectra of ethane-1,2-diol and other vicinal diols in benzene: GIAO/DFT shift calculations, Magn. Reson. Chem. 51 (2013) 32–41.
[27] B.C. Cabral, L. Albuquerque, F.S. Fernandes, Ab initio study of the conformational equilibrium of ethylene glycol, Theor. Chim. Acta 78 (1991) 271.
[28] P. Nagy, W. Dunn-III, G. Alagona, C. Ghio, Theoretical calculations on 1,2-ethanediol. Gauche-trans equilibrium in gas-phase and aqueous solution, J. Am. Chem. Soc. 113 (1991) 6719.
[29] C. Cramer, D. Thuhlar, Quantum chemical conformational analysis of 1,2-ethanediol: correlation and solvation effects on the tendency to form internal hydrogen bonds in the gas phase and in aqueous solution, J. Am. Chem. Soc. 116 (1994) 3892.
[30] L. Saiz, J. Padro, E. Guardia, Structure of liquid ethylene glycol: a molecular dynamics simulation study with different force fields, J. Chem. Phys. 114 (2001) 3187.
[31] N.C. Maiti, Y. Zhu, I. Carmichael, A.S. Serianni, V.E. Anderson, $^1J_{CH}$ correlates with alcohol hydrogen bond, J. Org. Chem. 71 (2006) 2878–2880.
[32] D.L. Crittenden, K.C. Thompson, M.J.T. Jordan, On the extent of intramolecular hydrogen bonding in gas-phase and hydrated eg, J. Phys. Chem. A 109 (2005) 2971–2977.
[33] D. Chopra, T.N.G. Rowa, E. Arunan, R.A. Klein, Crystalline ethane-1,2-diol does not have intra-molecular hydrogen bonding: experimental and theoretical charge density studies, J. Mol. Struct. 964 (2010) 126–133.
[34] C. Murli, N. Lu, Z. Dong, Y. Song, Hydrogen bonds and conformations in ethylene glycol under pressure, J. Phys. Chem. B 116 (2012) 12574.
[35] N. Zhang, W. Li, C. Chen, J. Zuo, L. Weng, Molecular dynamics study on water self-diffusion in aqueous mixtures of methanol, ethylene glycol and glycerol: investigations from the point of view of hydrogen bonding, Mol. Phys. 10 (2013) 1080.
[36] C. Møller, M.S. Plesset, Note on an approximation treatment for many-electron systems, Phys. Rev. 46 (1934) 0618–0622.
[37] J. Tomasi, B. Mennucci, R. Cammi, Quantum mechanical continuum solvation models, Chem. Rev. 105 (8) (2005) 2999–3094, http://dx.doi.org/10.1021/cr9904009.
[38] M.J. Frisch, G.W. Trucks, H.B. Schlegel, G.E. Scuseria, M.A. Robb, J.R. Cheeseman, G. Scalmani, V. Barone, B. Mennucci, G.A. Petersson, H. Nakatsuji, M. Caricato, X. Li, H.P. Hratchian, A.F. Izmaylov, J. Bloino, G. Zheng, J.L. Sonnenberg, M. Hada, M. Ehara, K. Toyota, R. Fukuda, J. Hasegawa, M. Ishida, T. Nakajima, Y. Honda, O. Kitao, H. Nakai, T. Vreven, J.A. Montgomery Jr., J.E. Peralta, F. Ogliaro, M. Bearpark, J.J. Heyd, E. Brothers, K.N. Kudin, V.N. Staroverov, R. Kobayashi, J. Normand, K. Raghavachari, A. Rendell, J.C. Burant, S.S. Iyengar, J. Tomasi, M. Cossi, N. Rega, J.M. Millam, M. Klene, J.E. Knox, J.B. Cross, V. Bakken, C. Adamo, J. Jaramillo, R. Gomperts, R.E. Stratmann, O. Yazyev, A.J. Austin, R. Cammi, C. Pomelli, J.W. Ochterski, R.L. Martin, K. Morokuma, V.G. Zakrzewski, G.A. Voth, P. Salvador, J.J. Dannenberg, S. Dapprich, A.D. Daniels,. Farkas, J.B. Foresman, J.V. Ortiz, J. Cioslowski, D.J. Fox, Gaussian 09 Revision B.01, Gaussian Inc. Wallingford CT, 2009.
[39] F. Jensen, The optimum contraction of basis sets for calculating spinspin coupling constants, Theor. Chem. Acc. 126 (5–6) (2010) 371–382, http://dx.doi.org/10.1007/s00214-009-0699-5.
[40] J.S. Lomas, ^{1}H NMR spectra of ethane-1,2-diol and other vicinal diols in benzene: GIAO/DFT shift calculations, Magn. Reson. Chem. 51 (1) (2013) 32–41, http://dx.doi.org/10.1002/mrc.3899.
[41] MonoEthyleneGlycol Global Company, Ethylene Glycol Product Guide, 2008. <http://www.meglobal.biz/product-literature>.
[42] D.P. Geerke, W.F. van Gunsteren, The performance of non-polarizable and polarizable force-field parameter sets for ethylene glycol in molecular dynamics simulations of the pure liquid and its aqueous mixtures, Mol. Phys. 105 (13–14) (2007) 1861–1881, http://dx.doi.org/10.1080/00268970701444631.
[43] A. Kaiser, O. Ismailova, A. Koskela, S.E. Huber, M. Ritter, B. Cosenza, W. Benger, R. Nazmutdinov, M. Probst, Ethylene glycol revisited: molecular dynamics simulations and visualization of the liquid and its hydrogen-bond network, J. Mol. Liq. 189 (0) (2014) 20–29 (fluid phase associations) http://dx.doi.org/10.1016/j.molliq.2013.05.033.
[44] R. Car, M. Parrinello, Unified approach for molecular dynamics and density-functional theory, Phys. Rev. Lett. 55 (1985) 2471–2474, http://dx.doi.org/10.1103/PhysRevLett.55.2471.
[45] Y.-L. Cheng, H.-Y. Chen, K. Takahashi, Theoretical calculation of the oh vibrational overtone spectra of 1-*n* alkane diols ($n = 24$): origin of disappearing hydrogen-bonded oh peak, J. Phys. Chem. A 115 (22) (2011) 5641–5653, http://dx.doi.org/10.1021/jp202030c.